JOURNAL OF APPLIED ELECTROCHEMISTRY 26 (1996) 487–491

Electrochemical investigation of Ni–P autocatalytic deposition in ammoniacal solutions

M. EBN TOUHAMI, M. CHERKAOUI, A. SRHIRI, A. BEN BACHIR
Ibn Tofail University, Faculty of Science, Kenitra, Morocco

E. CHASSAING
C.E.C.M–CNRS, 15 rue G. Urbain, 94407 Vitry-sur-Seine Cedex, France

Received 16 May 1995; revised 9 October 1995

The kinetics of Ni–P autocatalytic deposition in ammoniacal solutions was investigated by means of cyclic voltammetry and electrochemical impedance spectroscopy. The effect of the solution constituents (hypophosphite, nickel salt and pH) was examined. Strong interactions between the cathodic and anodic processes occur. The metal discharge is enhanced by the oxidation of hypophosphite, which is the predominant reaction in this process. The nickel deposition also affects the anodic process. With increasing pH the nickel discharge is progressively inhibited due to the change in the nature of the Ni(II) complexes. In contrast, in the presence of Ni(II) species, due to the opposite effect of the two partial processes, the plating rate increases for pH values up to 9 and then decreases for higher pH values.

1. Introduction

In previous work we have developed conditions for the preparation of Ni–Cu–P layers by autocatalytic deposition [1]. The deposits are compact and corrosion resistant. Their hardness can be increased up to 1000 Vickers by subsequent heat treatment. The structure, crystalline or amorphous, depends on the plating conditions, especially on the phosphorus content. Electrochemical investigation has identified the existence of strong interactions between the cathodic alloy discharge and the anodic oxidation of hypophosphite [2]. In addition, it has been shown that the reduction of cupric ions is partly controlled by diffusion and that an opposed variation exists between copper and phosphorus contents [2]. Aiming at a closer knowledge of the kinetics of the autocatalytic process, an investigation of the binary Ni–P system is first carried out.

Although Ni–P electroless deposition is a widely used commercial process, the deposition mechanism is still a matter of discussion. It is well known that the global process results from the anodic oxidation of the reducing agent and cathodic reactions, including metallic discharge, hydrogen evolution and phosphorus incorporation [3–15]. Complicated interactions between these reactions are known to occur [7, 8, 12].

2. Experimental procedure

The electrolyte composition was derived from the ternary alloy bath previously developed [1, 2]. It contained 0.5 M sodium hypophosphite, 0.05 M nickel sulfate, 0.2 M sodium citrate and 0.1 M ammonium acetate, the pH was adjusted to 9 by addition of ammonia. The temperature was held at $78 \pm 2^{\circ}$C. The solution was deaerated by nitrogen bubbling. The reference electrode was a saturated sulfate electrode (SSE). The counter electrode was a platinum sheet. Glassy carbon, nickel or mild steel discs were used as working electrodes. Prior to each experiment the electrodes were polished, degreased and etched in dilute sulfuric acid.

The effect of hypophosphite concentration (from 0.01 to 0.5 M) and nickel sulfate concentration (from 0.05 to 0.16 M) was investigated. The pH was varied between 8 and 10.5 by addition of ammonia.

A Solartron 1186 electrochemical interface coupled to a MacIntosh IIc microcomputer with home-made software, was used for cyclic voltammetry. The scan rate was varied from 5 to 200 mV s^{-1}. Two kinds of perturbations were applied: (i) the scan was started from the open-circuit potential E_0, the potential was decreased to the cathodic limit E_k, then increased to the anodic limit E_l and back to E_0; (ii) the scan was started from the anodic limit, E_l, down to the cathodic one, E_k, and back to the anodic potential E_l. Electrochemical impedance spectroscopy was carried out using a Solartron 1250 frequency response analyser at the deposition potential to estimate the plating rate.

The Ni–P layers deposited on steel were examined by scanning electron microscopy and their composition determined by energy dispersive X-ray spectroscopy.

3. Results

3.1. *Voltammetric investigation*

A voltammetric investigation was carried out, on stationary electrodes, to characterize the effect of the electrolyte constituents and their interactions.

0021-891X

Table 1. Influence of sodium hypophosphite concentration on the voltammetric characteristics (scan rate 20 mV s^{-1})

$H_2PO_2^-$ /M	Deposition		Peak A		Peak B		Peak C	
	E_k /V vs SSE	I_k /mA cm^{-2}	E_a /V vs SSE	I_a /mA cm^{-2}	E_b /V vs SSE	I_b /mA cm^{-2}	E_c /V vs SSE	I_c /mA cm^{-2}
0.00	−1.60	−55			−0.83	4.0		0.0
0.01	−1.60	−51			−0.76	4.4	−0.115	4.8
0.10	−1.60	−76	−1.20	3.1	−0.77	4.9	0.025	10.6
0.25	−1.60	−80	−1.19	6.6	−0.79	4.1	−0.013	9.8
0.35	−1.60	−94	−1.20	6.6	−0.77	4.4	0.017	12.6
0.50	−1.60	−100	−1.16	14.0	−0.79	5.3	−0.020	15.0

3.1.1. Effect of hypophosphite and nickel sulfate concentrations. Figure 1 shows the voltammograms recorded at 20 mV s^{-1} for various hypophosphite concentrations on a vitreous carbon electrode. On the forward scan, from −1.3 to −1.6 V, the cathodic deposition of Ni–P alloy is observed. The deposition is depolarised when the hypophosphite concentration is increased (Fig. 1) and the current, I_k, at the upper cathodic limit, $E_k = -1.60$ V vs SSE, increases linearly with hypophosphite concentration (Fig. 2, Table 1). This indicates that hypophosphite has a marked effect on the cathodic process: it enhances the nickel discharge and eventually hydrogen evolution as already observed for Ni–Cu–P deposition [2]. On the reverse scan three oxidation peaks are usually observed, denoted A, B and C (Fig. 1, curve 3). In the absence of hypophosphite, only peak B occurs (Fig. 1, curve 1). This can then be related to the oxidation of crystalline nickel, in agreement with other observations [14, 16]. Peak A is observed for hypophosphite concentrations larger than 0.1 M. The peak intensity, I_a, increases with hypophosphite concentration (Fig. 2). It is associated with the oxidation of hypophosphite, as already reported [8]. Peak C occurs only when the electrolyte contains both hypophosphite and nickel salts. Its intensity increases linearly with hypophosphite concentration. This peak is attributed to the oxidation of a P-rich Ni–P phase [12–15, 16].

The effect of nickel sulfate concentration is not very pronounced (Table 2). The potential, E_a, of peak A is slightly shifted towards less negative potential and I_a is slightly enhanced. The increase in nickel sulfate concentration does not change the deposition current markedly, I_k, at the upper cathodic limit ($E_k = -1.56$ V vs SSE). The intensity of peak B and peak C increase slightly.

The effect of these two constituents demonstrates the existence of strong interactions between the cathodic and the anodic processes. The reduction of nickel sulfate increases the hypophosphite oxidation and the presence of hypophosphite enhances the nickel discharge.

3.1.2. Effect of electrolyte pH. The pH was increased from 8 to 10.5 by addition of ammonia. The deposition current I_k at the cathodic limit $E_k = -1.56$ V vs SSE, is markedly decreased from 75 mA cm^{-2} to 10 mA cm^{-2}, indicating that the

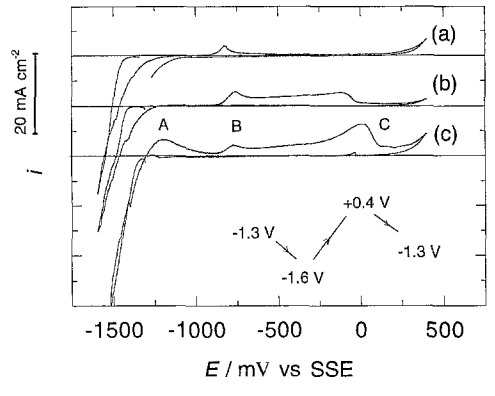

Fig. 1. Cyclic voltammogram recorded on glassy carbon electrode for various hypophosphite concentrations. Scan rate: 20 mV s^{-1}, (a) No hypophosphite, (b) 0.01 M hypophosphite, and (c) 0.35 M hypophosphite.

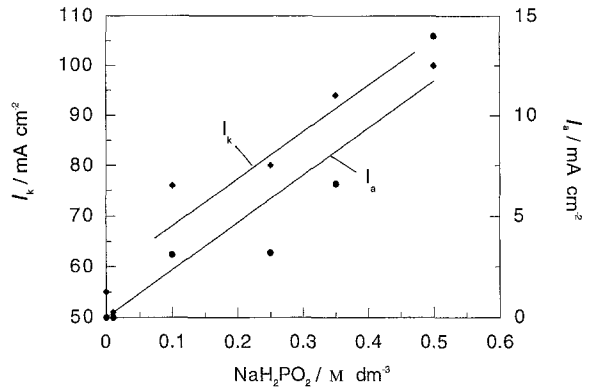

Fig. 2. Deposition current, I_k, at upper cathodic limit ($E_k = -1.6$ V vs SSE) and anodic peak current, I_a, as a function of hypophosphite concentration.

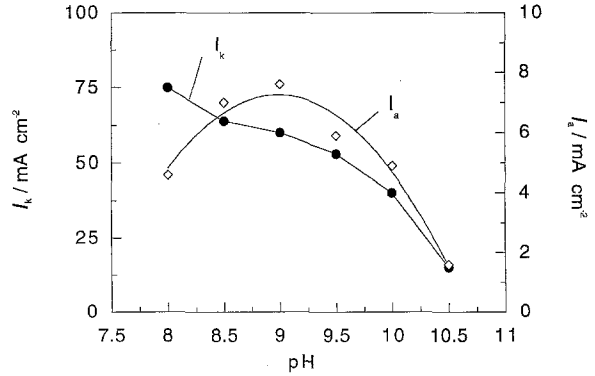

Fig. 3. pH dependence of deposition current, I_k, at upper cathodic limit ($E_k = -1.56$ V vs SSE), and anodic peak current, I_a.

Table 2. Influence of nickel sulfate concentration on the voltammetric characteristics (scan rate 20 mV s^{-1})

$NiSO_4$ /M	Deposition		Peak A		Peak B		Peak C	
	E_k /V vs SSE	I_k /mA cm^{-2}	E_a /V vs SSE	I_a /mA cm^{-2}	E_b /V vs SSE	I_b /mA cm^{-2}	E_c /V vs SSE	I_c /mA cm^{-2}
0.05	−1.56	−60	−1.22	7.3	−0.790	2.4	−0.056	2.5
0.10	−1.56	−61	−1.20	7.6	−0.785	3.2	−0.063	5.2
0.16	−1.56	−62	−1.18	8.6	−0.775	3.4	−0.068	5.4

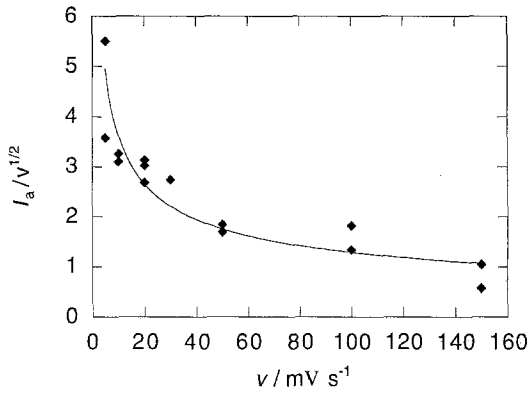

Fig. 4. Potential sweep function for peak A ($I_a/v^{1/2}$) as a function of scan rate, v.

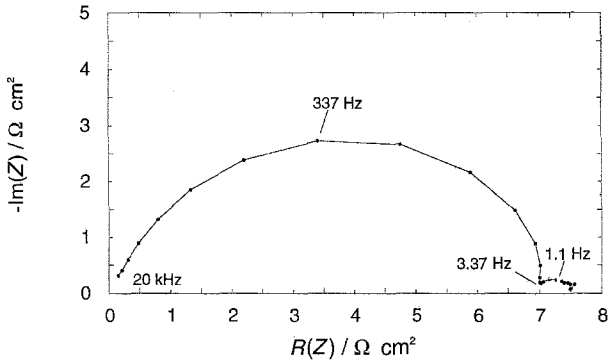

Fig. 5. Electrochemical impedance plot recorded at the deposition potential E_d = −1.34 V vs SSE, mild steel disc electrode rotating at 500 rpm, in standard electrolyte.

nickel discharge process becomes increasingly inhibited (Fig. 3). This feature may be related to the change of nickel complexes, since the citrate–amino-nickel complexes are more difficult to reduce than citrate–nickel species [15]. On the reverse scan the intensity of peak A, I_a, increases when the pH is increased from 8 to 9 and then decreases (Fig. 3). This results from the competition of two opposite reactions. The peak potential E_a shows a linear pH dependence with a slope equal to 52 mV per pH unit.

3.1.3. Effect of scan rate (5–200 mV s^{-1}). The potential of peak A does not change markedly with scan rate, v. I_a increases with increasing rate up to 100 mV s^{-1} and then decreases slightly. By plotting $I_a/v^{1/2}$ as a function of v a continuous decrease is observed (Fig. 4). This is a diagnostic criterion for a kinetic scheme where chemical reaction precedes charge transfer [17, 18].

Peak B is observed only for rates larger than 10 mV s^{-1}. Its intensity increases with scan rate but its potential remains nearly constant. Intensities of peak C and peak A vary in an opposite way.

3.1.4. Effect of the substrate nature. The voltammograms recorded on mild steel or nickel are similar to those obtained with glassy carbon. However, the deposition current, I_k, and the hypophosphite oxidation current, I_a, are larger on glassy carbon than on the metallic electrodes (Table 3). The potential of peak C, E_c, corresponding to the dissolution of a P rich Ni–P phase is more positive. This shift may be related to the lower hydrogen content of the alloys deposited on nickel and especially on mild steel, in which occluded hydrogen may penetrate.

Table 3. Influence of the electrode nature on the voltammetric characteristics (v = 10 mV s^{-1})

	Mild steel	Nickel	Glassy carbon
I_a/mA cm^{-2}	4.5	3.4	9.5
I_k/mA cm^{-2}	45	60	100
E_c/mV vs SSE	245	170	65

3.2. *Electrochemical impedance at the deposition potential*

Figure 5 shows an example of an impedance diagram recorded at the deposition potential, E_d. The high frequency loop is related to the relaxation of the double layer capacitance (in the range 50–100 μF cm^{-2}) in parallel with the charge transfer resistance, R_t, which is inversely proportional to the plating rate [3]. An additional low-frequency capacitive feature is also observed related to adsorption processes or to a multistep reaction.

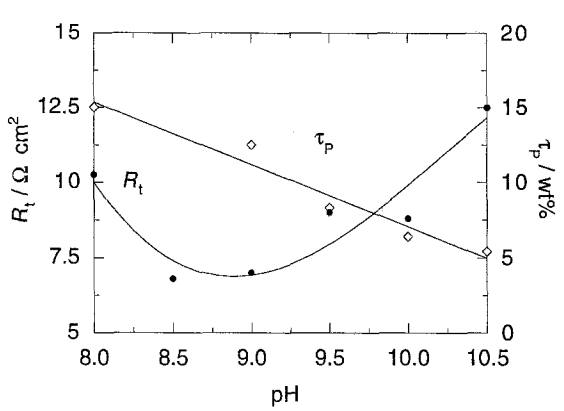

Fig. 6. pH dependence of charge transfer resistance, R_t, and phosphorus content in the deposit, τ_P.

Table 4. Influence of the electrode rotation speed on the deposition potential E_d, the phosphorus content τ_P and the charge transfer resistance R_t

Ω/rpm	0	500	1000
τ_P/wt %	13	12.5	13
E_d/mV vs SSE	−1365	−1340	−1340
R_t/Ω cm^2	12	7	7

The working electrode was a mild steel disc rotating at up to 1000 rpm. The charge transfer resistance, R_t, decreases as the rotation speed increases from 0 to 500 rpm. No further variation is observed for larger speeds (Table 4). In the following the impedance diagrams are recorded at 500 rpm.

The charge transfer resistance, R_t, is markedly decreased, when the hypophosphite concentration is increased from 0.1 to 0.5 M (Table 5) or when the nickel sulfate concentration is increased from 0.05 to 1.6 M (Table 6). When the pH is raised from 8 to 10.5 the charge transfer resistance exhibits a minimum (Fig. 6).

3.3. *Influence of the plating condition on the deposit composition*

At the deposition potential, E_d, and for a pH value of 9, the phosphorus content in the deposit τ_P is equal to 12.5 ± 0.5 wt % (Table 4), whatever the electrode rotation speed. The incorporation reaction is not a diffusion controlled process. It increases only slightly from 11 to 13 wt %, when the hypophosphite concentration is increased from 0.1 to 0.5 M (Table 5) and it decreases with increasing nickel sulfate concentration from 0.05 to 0.16 M (Table 6) or when the pH is increased from 8 to 10.5 (Fig. 5).

4. Discussion

The electroless process results from the anodic oxidation of the reductant (here hypophosphite) and the cathodic reduction. The anodic oxidation of hypophosphite is the dominant factor in electroless deposition [7, 8]. Indeed, the plating rate $1/R_t$ and I_a the anodic peak current are proportional (Fig. 7). The scan rate variation of the potential sweep function, $I_a/v^{1/2}$ (Fig. 4) indicates that a chemical reaction preceeds charge transfer [17, 18]. This is probably a deprotonation reaction, which can be written as

$$H_2PO_2^- \longrightarrow HPO_2^- + H_{ads} \qquad (1)$$

This reaction occurs only on a catalytic surface [5, 7], here the Ni–P growing layer. A rearrangement of hypophosphite anion would occur on the surface [5]: Two different interactions with the catalytic surface

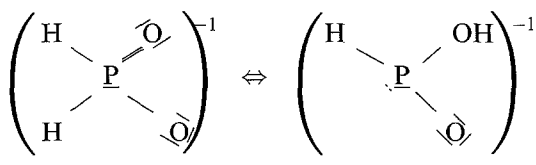

Table 5. Influence of hypophosphite concentration on the deposition potential E_d, the phosphorus content τ_P and the charge transfer resistance R_t

NaH_2PO_2/M	0.1	0.2	0.35	0.5
E_d/mV vs SSE	−1318	−1290	−1330	−1340
R_t/Ω cm^2	23.5	10	8.6	7
τ_P/wt %	11.75	11	12.5	12.5

Table 6. Influence of nickel sulfate concentration on the deposition potential E_d, the phosphorus content τ_P and the charge transfer resistance R_t

$NiSO_4$/M	0.05	0.1	0.16
E_d/mV vs SSE	−1340	−1235	−1230
R_t/Ω cm^2	7	5.4	2.5
τ_P/wt %	12.5	7.9	7.5

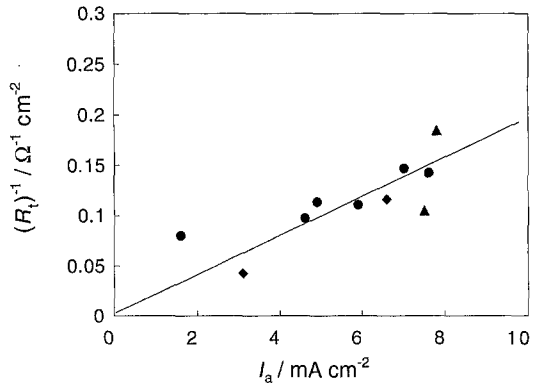

Fig. 7. Inverse of the charge transfer resistance, $1/R_t$, as a function of anodic peak current, I_a, for different conditions: (●) pH variation from 8 to 10.5; (◆) variation of hypophosphite concentration (0–0.5 M); (▲) variation of nickel sulfate concentration (0.5–0.16 M).

have been considered: the hypophosphite binds to the surface through the P atom [9, 12] or through hydrogen bonds [7, 10] and then deprotonates. However, it has been shown that no simple correlation exists between the order of the catalytic activity of the metals for the hydrogen electrode reaction and that for the anodic oxidation of the reducing agent [8].

The voltammograms have, in the anodic range of peak A (Fig. 1) a 'volcano type' shape [7, 8]. The polarization curve is similar to those obtained for the passivation of metals or alloys. However, the depression of current occurs at potentials more negative than that for the formation of metal oxides. This is probably connected with the adsorption of a blocking species, which may be a hydroxide compound as suggested by Ohno [8]. A reaction path derived from those developed for passivation reactions can be considered to be

$$(HPO_2)^-_{surf} + OH^- \longrightarrow (HPO_2OH)^-_{solution} + e^- \qquad (2)$$

$$(NaHPO_2)_{surf} + nOH^- \Leftrightarrow [NaHPO_2(OH)_n]_{ads} + ne^- \qquad (3)$$

where $[NaHPO_2(OH)_n]_{ads}$ adsorbs and blocks the electrode area.

This scheme accounts for the increase in the peak

current, I_a, with hypophosphite concentration (Table 1). In the absence of metallic species I_a increases continuously with pH [7]. The decrease observed at pH values larger than 9 (Fig. 2) is then attributed to interactions with the cathodic nickel discharge which is inhibited by pH increase. Such a reaction scheme in which Reaction 2 has an activation coefficient with potential smaller than that of Reaction 3 generates the 'volcano type' shape of the curve. It is not necessary to involve several blocking adsorbates as proposed by Ohno [8].

The cathodic processes include nickel discharge, phosphorus incorporation, and hydrogen evolution and its eventual incorporation into the deposit. Phosphorus incorporation results from a reduction of hypophosphite ions, according to

$$H_2PO_2^- + e^- \longrightarrow P + 2OH^- \quad (4)$$

This is not a major reaction since the P content in the deposit is about 21 at %. The predominant reaction is the nickel discharge from complexed citrate–ammonia nickel species, written as Ni(II) to simplify. The global reaction may be written as

$$Ni(II) + 2e^- \longrightarrow Ni \quad (5)$$

The reduction of the nickel species is inhibited by a pH increase probably because of the formation of amino complexes which are more stable than the citrate complex [15]. These reactions account for a decrease of P content with increasing nickel sulfate concentration or pH, an increase of P content with hypophosphite content.

In addition hydrogen is evolved and may be incorporated into the deposit, according to:

$$2H^+ + 2e^- \longrightarrow H_2 \quad (6)$$

$$H^+ + e^- \longrightarrow H_{included} \quad (7)$$

The interactions between anodic and cathodic processes are probably generated through Reaction 1 corresponding to the deprotonation reaction of the hypophosphite anion. This reaction is driven to the right both by the anodic and the cathodic processes. This is evident for the oxidation of hypophosphite. For the cathodic process it is likely that there exists a coupling between Ni(II) discharge and hydrogen. The electrocrystallization of nickel has been mainly investigated in acid solutions [19, 20]. In sulfate electrolyte it has been shown that interactions between nickel and hydrogen discharge occur [20]. The process is probably somewhat different in alkaline solutions. However, the voltammograms recorded on various substrates point out the role of hydrogen in the plating process (Table 3). Both the oxidation and the discharge currents are larger on glassy carbon electrodes, where H_{ads} produced by Reaction 1, cannot penetrate into the substrate, than on nickel or mild steel.

5. Conclusion

Voltammetric and electrochemical impedance measurements confirm that strong interactions occur between the anodic and the cathodic processes, probably through deprotonation of the hypophosphite anion which occurs on the catalytic surface of the growing layer. The impedance results confirm that the anodic process controls the plating rate.

Acknowledgement

This investigation was carried out as part of a French–Moroccan InterUniversity Cooperation Grant (grant 94/786).

References

[1] M. Cherkaoui, A. Srhiri and E. Chassaing, *Plat. Surf. Finish.* **79** (1992) 68.
[2] E. Chassaing, M. Cherkaoui and A. Srhiri, *J. Appl. Electrochem.* **23** (1993) 1169.
[3] C. Gabrielli and F. Raulin, *ibid.* **1** (1971) 167.
[4] C. H. De Minjer, *Electrodeposition & Surf. Treat.* **3** (1975) 261.
[5] J. H. Marshall, *J. Electrochem. Soc.* **130** (1983) 369.
[6] J. Bielinski, *Oberfläche-Surface* **25** (1984) 423.
[7] I. Ohno, O. Wakabayashi and S. Haruyama. *J. Electrochem. Soc.* **132** (1985) 2323.
[8] I. Ohno, *Mater. Sci. Eng. A* **146** (1991) 33.
[9] V. F. Makarov, Yu. V. Prusov and V. N. Flerov, *Elektrokhimiya* **26** (1990) 858.
[10] Z. Jusys, J. Liaukonis and A. Vaskelis, *J. Electroanal. Chem.* **307** (1991) 87.
[11] L. D. Burke and B. H. Lee, *J. Appl. Electrochem.* **22** (1992) 48.
[12] A. H. Gafin and S .W. Orchard, *J. Electrochem. Soc.* **140** (1993) 3458.
[13] E. C. Pereira and S. Wolynec, *Met. Finish.* **81**(4) (1993) 45.
[14] U. Hofmann and K. G. Weil, *Dechema-Monographien* **121** (1990) 257.
[15] L. M. Abrantes and J. P. Correia, *J. Electrochem. Soc.* **141** (1994) 2356.
[16] J. Crousier, Z. Hanane, J.-P. Crousier, *Electrochim. Acta* **38** (1993) 261.
[17] R. S. Nicholson and I. Shain, *Anal. Chem.* **36** (1964) 706.
[18] R. Greef, R. Peat, L. M. Peter, D. Pletcher and J. Robinson, *in* 'Instrumental Methods in Electrochemistry', Ellis Horwood (1990) pp. 178–191.
[19] I. Epelboin, M. Joussellin and R. Wiart, *J. Electroanal. Chem.* **119** (1981) 61.
[20] E. Chassaing, M. Joussellin and R. Wiart, *ibid.* **157** (1983) 75.